Anisotropic Acoustodynamics in Gigahertz Piezoelectric Ultrasonic Transducers

Jingjie Cheng, Zhaoliang Peng, Penghui Song, Bo Peng, Jason J. Gorman, Justin Kuo, Amit Lal, Wenming Zhang, and Lei Shao

***Abstract*—In this work, we employed our newly developed optical imaging method to probe detailed acoustodynamic physics in gigahertz unreleased ultrasonic transducers based on an AlN-on-silicon system, revealing mode superposition, anisotropic transduction, and dynamic mode evolution. Superpositioned upon the dominant breathing mode along the vertical direction of the AlN layer, multiple resonant lateral modes are identified, and they are shown to evolve into a surface mode beyond the piezoelectric transduction envelope, with strong anisotropic transduction brought by the shear motion of silicon. This acoustodynamic property is important for verifying and further improving design theories of broadband piezoelectric transducers and thin film piezoelectric-on-substrate systems in general.**

***Index Terms*—Piezoelectric micromachined ultrasonic transducers (PMUTs), acoustodynamics, gigahertz ultrasonics, superposition, anisotropy.**

I. Introduction

PIEZOELECTRIC micromachined ultrasonic transducers (PMUTs) have attracted significant attention due to their important roles in applications such as biomedical imaging [1]−[4] and temperature sensing [5], [6]. They typically consist of a released piezoelectric thin-film material, such as aluminum nitride (AlN) [7]−[14] or lead zirconate titanate (PZT) [15]−[19] and are an ideal solution for integrated transducer arrays with high frequencies and bandwidth. Research has focused on quality factor optimization [8], anchored boundary structures [10], electrode geometric design [14], and airborne coupling [17] to improve their performance. These design methods tailor the vibrational mode shapes of the devices for specific applications and have received considerable attention through simulation studies and experimental validation [7], [9].

Recent results have demonstrated micrometer-thick unreleased piezoelectric transducers to raise the detection frequency to gigahertz and eliminate the need for released membranes, leading to a much higher imaging resolution and significantly improved packaging reliability, respectively [2], [3], [20], [21]. These gigahertz solidly-mounted PMUTs (SM-PMUTs) exhibit acoustodynamic behaviors that are not well studied due to the lack of techniques for characterizing their complex physics at microwave frequencies. This impedes their further optimization since modeling their acoustodynamics is critical for understanding energy dissipation sources, undesirable resonances, and their device performance in general.

Here, we study the dynamic behavior of SM-PMUTs out to 4 GHz relying on super high frequency mapping of acoustic wavefields using recently-developed femtosecond laser interferometry [22], which reveals complex ultrasonic superposition, anisotropy, and mode evolution at microwave frequencies. The mode dispersion and evolution over a wide frequency range are particularly important for the design of broadband ultrasonic devices. It opens a path to identifying spurious responses and refining their designs for high-frequency specifications, which is beneficial to the development of PMUTs and other next-generation piezoelectric ultrasonics.

II. Results and Discussion

The SM-PMUT device studied here (Fig. 1(a)) consists of an AlN thin film sandwiched between two metal layers fabricated on a double-side polished silicon substrate. These multi-layer devices were fabricated on a 725 μm thick oxide-coated silicon substrate with patterned molybdenum (Mo) layer as its bottom electrode. A 2 μm AlN layer was then sputtered and patterned by reactive ion etching, followed by top Mo electrode deposition and then oxide passivation. A cross-sectional diagram of the layer stack with nominal thickness is shown in Fig. 1(b). Ultrasonic waves and resonances are excited in the piezoelectric layer by d_{33} transduction along the thickness direction.

We first perform electrical characterization of the fabricated SM-PMUT. As shown in Fig. 1(c), the S11 spectrum exhibits a primary resonance around 2.4 GHz, consistent with the fundamental breathing mode of the 2 μm AlN piezoelectric

Manuscript received XX; revised XX; accepted XX. Date of publication XX; date of current version XX. This work was supported in part by the National Science Foundation for Young Scientists of China under Grant 12002201, in part by the Program of Shanghai Academic/Technology Research Leader of China under Grant 19XD1421600, in part by the Shanghai Sailing Program of Shanghai Science and Technology Committee of China under Grant 19YF1425000, and in part by the SJTU Global Strategic Partnership Fund (2021 SJTU-CORNELL). (*Corresponding author: Lei Shao.*)

Jingjie Cheng, Zhaoliang Peng and Lei Shao are with the University of Michigan-Shanghai Jiao Tong University Joint Institute, Shanghai Jiao Tong University, Shanghai 200240, China (e-mail: lei.shao@sjtu.edu.cn).

Penghui Song, Bo Peng and Wenming Zhang are with the School of Mechanical Engineering and State Key Laboratory of Mechanical Systems and Vibration, Shanghai Jiao Tong University, Shanghai 200240, China.

Jason J. Gorman is with the National Institute of Standards and Technology, Gaithersburg, Maryland 20899, USA.

Justin Kuo and Amit Lal are with Electrical and Computer Engineering, Cornell University, Ithaca, New York 14853, USA.

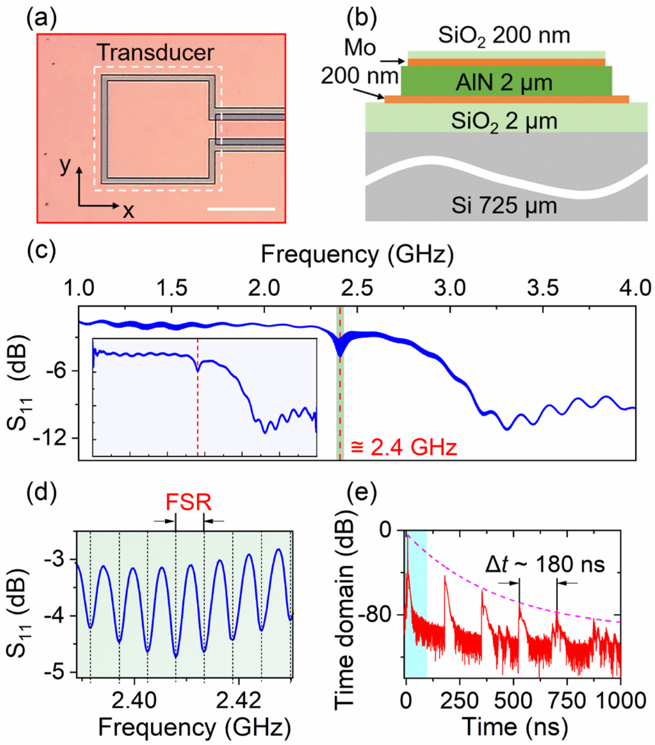

Fig. 1. (a) Optical micrograph of the device under test with the scale bar indicating 50 μm. (b) Schematic cross-sectional diagram of material layers with corresponding nominal thicknesses. (c) Electromechanical S11 spectrum of the SM-PMUT from 1 GHz to 4 GHz. Time gating from -10 ns to 100 ns is applied to this signal, resulting in a clean S11 spectrum shown as the inset. (d) Magnified S11 spectrum for the green shaded window in (c). (e) The time-domain electrical response of the device resulting from the inverse Fourier transform of the S11 spectrum.

transducer along the thickness direction. The signal reduction at higher frequencies is due to uncompensated cable, packaging, and network analyzer attenuation. There are a series of dense, equidistant resonant phonon modes of the 725 μm thick silicon cavity in the proximity of the 2.4 GHz primary resonance, where the free spectral range is approximately 5.8 MHz, as shown in Fig. 1(d). In addition, the time-domain electrical response of the device yielded from the inverse Fourier transform of the S11 spectrum, shown in Fig. 1(e), exhibits a series of echoes that exponentially decay in amplitude (marked with magenta dotted line). The time interval between these echoes is near 180 ns, which agrees with the expected travel time of an ultrasonic pulse making a round trip inside the silicon substrate. In order to show that these dense resonant dips are the cavity modes of the silicon substrate, we apply a time gating from -10 ns to 100 ns (light cyan shaded area) to the S11 spectrum to remove all echoes reflected from the other side of the silicon, resulting in a clean S11 spectrum (inset in Fig. 1(c)) showing only the primary resonance near 2.4 GHz.

Dynamic optical imaging of the gigahertz SM-PMUTs provides direct visualization of the complete acoustic wavefields. Using our recently developed femtosecond laser interferometry [22], we are the first to map vibrational mode profiles out to 4 GHz under a high signal-to-noise ratio while the SM-PMUTs are driven under normal sinusoidal electrical signals. The amplitude and phase mappings at 2.4 GHz are displayed in Figs. 2(a)–2(b). A 3D view of the displacement field is thus reconstructed in Fig. 2(c), where lateral modes along the *x*- and *y*- directions are superimposed upon the piston-like motion of the primary mode, and the energy leakage of the acoustic waves is visible through its signal trace to the right.

To study these shear modes, we extract the cross-sectional displacement profiles from the 3D mappings along the *x*- and *y*-directions from 2.1 GHz to 3.0 GHz. These profiles are stacked in Figs. 2(d)–2(e) with the result along the *x*-direction

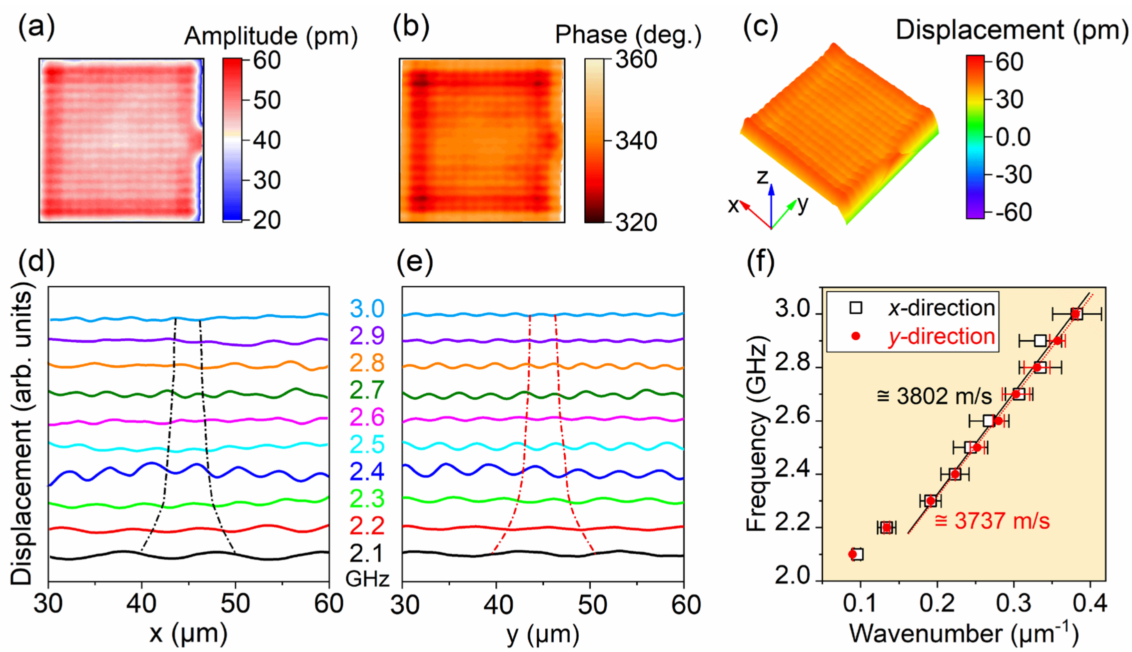

Fig. 2. Optical characterization of the SM-PMUTs. (a), (b) The amplitude and phase mappings of the vibrational wavefield of the fundamental resonance at 2.4 GHz. (c) A three-dimensional view of the acoustic displacement by combining amplitude and phase mappings. Extraction of the cross-sectional displacement profiles from the 3D mappings along the *x*- and *y*-directions at frequencies below, at, and above the fundamental mode from 2.1 GHz to 3.0 GHz is shown in (d) and (e), respectively. (f) The acoustic dispersion diagram for the lateral modes along the *x*- and *y*-directions, with the error bars representing +/- one standard deviation.

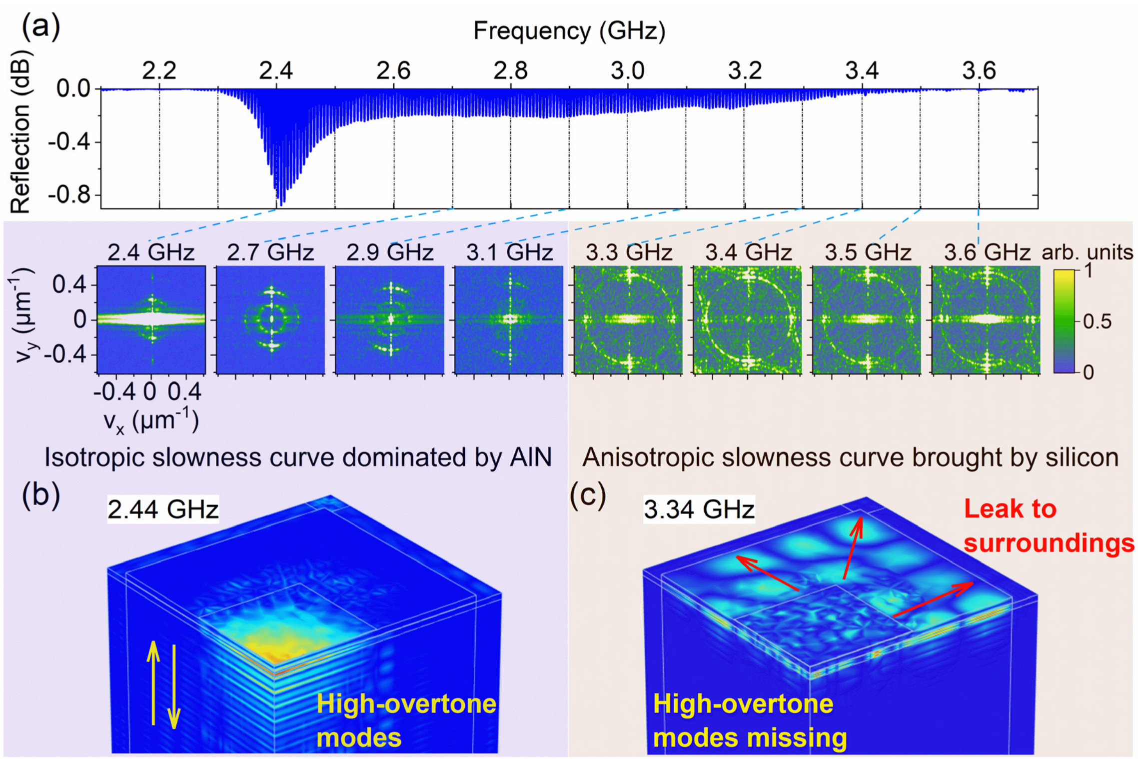

Fig. 3. (a) Extraction of the high-overtone modes by removing the slowly-varying envelope in the S11 spectrum. Spatial 2D-FFT for the optical acoustic mappings for a series of selected frequencies yields images of the acoustic modes as a function of wavenumbers along the *x*- and *y*-directions. (b), (c) Finite element analysis for a quarter of the device at 2.44 GHz and at 3.34 GHz, respectively.

amplified by 5 times due to energy loss. It shows periodicity along both directions, featuring standing waves as high-order shear modes in the AlN transducer. In addition, the periodicity (equal to wavelength, λ) gradually decreases as a function of frequency. We then calculate the wavenumbers ($1/\lambda$) and obtain the dispersion in Fig. 2(f) with the uncertainty obtained by multiple reading of the period in Figs. 2(d) and 2(e), showing a mostly linear relationship. The acoustic shear velocities along the x- and y-directions are found to be close for larger wavenumber, indicating isotropic transduction.

Next, we investigate the broadband dynamic interaction between the AlN transduction and the silicon cavity modes. In such material systems, the energy of the main AlN transduction mode is injected into the substrate cavity and serves as the transduction envelope to select those high-overtone cavity modes that can be practically excited. These modes are shown by removing the slowly-varying AlN transduction envelope (inset in Fig. 1(c)) from the S11 spectrum (Fig. 1(c)), revealing a comb of dense high-overtone bulk acoustic resonances inside the first transduction envelope, which are maximized around 2.4 GHz and gradually disappear around 3.4 GHz (Fig. 3(a)).

We perform spatial 2D fast Fourier transform (2D-FFT) upon the acoustic mappings for a series of selected frequencies, both inside and outside of the first transduction envelope. This yields images of the acoustic modes as a function of wavenumbers along the x- and y-directions. Circular symmetric modes concerning the XY-plane can be observed at all these frequencies, and show gradually enlarged radius as increasing frequency, resulted from the decrease in wavelength for the shear modes described above. Such a circular shape is on account of the isotropic symmetry of all the mode wave velocities in the AlN layer, demonstrating the dominant AlN transduction. Interestingly, at frequencies of (3.3, 3.4, 3.5, and 3.6) GHz, the apparent non-circular symmetry (resembling four-leaf clovers) shows up in the 2D-FFT diagrams, which means that the acoustic velocities of certain lateral modes become anisotropic, which is the result of the shear modes of the silicon substrate.

According to the power spectrum of the dense silicon cavity modes, the onset frequency of this anisotropy is near 3.3 GHz, which is at the edge of the transduction envelope. It is clear that at around 3.3 GHz the power of the teeth inside the comb becomes much smaller than that of the peak value and eventually vanishes. In fact, these modes significantly leak into the passive area as propagating waves beyond 3.3 GHz, as shown in Figs. 3(b)−3(c). Finite element analysis confirms the efficient generation of vertical cavity modes at 2.44 GHz (inside the transduction envelope), while not actuated at 3.34 GHz (outside of this envelope). Instead, the resonant shear modes evolve into leaking surface acoustic waves.

III. Conclusion

In summary, we demonstrate the broadband acoustodynamic behaviors of AlN-based gigahertz SM-PMUTs including multiple mode superposition, anisotropic transduction and dynamic mode evolution, by means of optical mappings of vibrational wavefields out to 4 GHz. These GHz acoustodynamics provide guidelines for improving the simulation models and dynamics design for future work.

REFERENCES

[1] Y. Lu, H. Tang, S. Fung, Q. Wang, J. M. Tsai, M. Daneman, B. E. Boser, D. A. Horsley, "Ultrasonic fingerprint sensor using a piezoelectric micromachined ultrasonic transducer array integrated with complementary metal oxide semiconductor electronics," *Appl. Phys. Lett.,* vol. 106, no. 26, Jun. 2015, Art no. 263503, doi: 10.1063/1.4922915.

[2] J. Hoople, J. Kuo, M. Abdel-moneum, and A. Lal, "Chipscale GHz Ultrasonic Channels for Fingerprint Scanning," in *2015 IEEE International Ultrasonics Symposium (IUS)*, Taipei, Taiwan, Oct. 2015, pp. 1-4, doi: 10.1109/ULTSYM.2015.0027.

[3] J. C. Kuo, J. T. Hoople, M. Abdelmejeed, M. Abdel-moneum, and A. Lal, "64-Pixel Solid State CMOS Compatible Ultrasonic Fingerprint Reader," in *IEEE 30th International Conference on Micro Electro Mechanical Systems (MEMS)*, Las Vegas, NV, USA, Jan. 2017, pp. 9-12, doi: 10.1109/MEMSYS.2017.7863326.

[4] X. Jiang, H. Y. Tang, Y. Lu, E. J. Ng, J. M. Tsai, B. E. Boser, D. A. Horsley, "Ultrasonic Fingerprint Sensor With Transmit Beamforming Based on a PMUT Array Bonded to CMOS Circuitry," *IEEE Trans. Ultrason. Ferroelectr. Freq. Control,* vol. 64, no. 9, pp. 1401-1408, Sep. 2017, doi: 10.1109/TUFFC.2017.2703606.

[5] M. Abdelmejeed, J. C. Kuo, and A. Lal, "Thermal wavefront imaging using GHz ultrasonics," in *2017 IEEE International Ultrasonics Symposium (IUS)*, Washington, DC, USA, Sept. 2017, pp. 1-4, doi: 10.1109/ULTSYM.2017.8092655.

[6] M. Abdelmejeed, J. C. Kuo, and A. Lal, "A CMOS compatible GHz ultrasonic pulse phase shift based temperature sensor," in *2018 IEEE Micro Electro Mechanical Systems (MEMS)*, Belfast, UK, Jan. 2018, pp. 1108-1111, doi: 10.1109/MEMSYS.2018.8346754.

[7] T. Wang, R. Sawada, and C. Lee, "A Piezoelectric Micromachined Ultrasonic Transducer Using Piston-Like Membrane Motion," *IEEE Electron Device Lett.,* vol. 36, no. 9, pp. 957-959, Jul. 2015, doi: 10.1109/led.2015.2459075.

[8] X. Chen, X. Liu, T. Wang, X. Le, F. Ma, C. Lee, J. Xie, "Piezoelectric micromachined ultrasonic transducers with low thermoelastic dissipation and high quality factor," *J. Micromech. Microeng.,* vol. 28, no. 5, Mar. 2018, Art no. 057001, doi: 10.1088/1361-6439/aab1bc

[9] X. Chen, D. Chen, X. Liu, D. Yang, J. Pang, and J. Xie, "Transmitting Sensitivity Enhancement of Piezoelectric Micromachined Ultrasonic Transducers via Residual Stress Localization by Stiffness Modification," *IEEE Electron Device Lett.,* vol. 40, no. 5, pp. 796-799, Mar. 2019, doi: 10.1109/led.2019.2904293.

[10] Y. Liang, B. Eovino, and L. Lin, "Piezoelectric Micromachined Ultrasonic Transducers With Pinned Boundary Structure," *J. Microelectromech. Syst.,* vol. 29, no. 4, pp. 585-591, Aug. 2020, doi: 10.1109/jmems.2020.3001560.

[11] Y, Fu, S. Sun, Z. Wang, P. Niu, M. Zhang, S. Chen, W. Pang, "Piezoelectric Micromachined Ultrasonic Transducer With Superior Acoustic Outputs for Pulse-Echo Imaging Application," *IEEE Electron Device Lett.,* vol. 41, no. 10, pp. 1572-1575, Aug. 2020, doi: 10.1109/led.2020.3018310.

[12] Z. Tong, H. Hu, Z. Wu, S. Xie, G. Chen, S. Zhang, L. Lou, H. Liu, "An Ultrasonic Proximity Sensing Skin for Robot Safety Control by Using Piezoelectric Micromachined Ultrasonic Transducers (PMUTs)," *IEEE Sensors J.,* Mar. 2021, doi: 10.1109/jsen.2021.3068487.

[13] X. Chen, M. Qu, K. Zhu, and J. Xie, "Dual-Frequency Piezoelectric Micromachined Ultrasonic Transducers via Beam-Membrane Coupled Structure," *IEEE Electron Device Lett.,* vol. 42, no. 6, pp. 919-922, Apr. 2021, doi: 10.1109/led.2021.3075853.

[14] L. Jia, L. Shi, C. Liu, C. Sun, and G. Wu, "Enhancement of Transmitting Sensitivity of Piezoelectric Micromachined Ultrasonic Transducers by Electrode Design," *IEEE Trans. Ultrason. Ferroelectr. Freq. Control,* vol. 68, no. 11, pp. 3371-3377, Nov. 2021, doi: 10.1109/TUFFC.2021.3087741.

[15] T. Wang, T. Kobayashi, and C. Lee, "Micromachined piezoelectric ultrasonic transducer with ultra-wide frequency bandwidth," *Appl. Phys. Lett.,* vol. 106, no. 1, Jan. 2015, Art no. 013501, doi: 10.1063/1.4905441.

[16] S. Sadeghpour, M. Kraft, and R. Puers, "Design and fabrication strategy for an efficient lead zirconate titanate based piezoelectric micromachined ultrasound transducer," *J. Micromech. Microeng.,* vol. 29, no. 12, Oct. 2019, Art no. 125002, doi: 10.1088/1361-6439/ab4527.

[17] G.-L. Luo, Y. Kusano, and D. A. Horsley, "Airborne Piezoelectric Micromachined Ultrasonic Transducers for Long-Range Detection," *J. Microelectromech. Syst.,* vol. 30, no. 1, pp. 81-89, Feb. 2021, doi: 10.1109/jmems.2020.3037298.

[18] S. Tiwari, R. Kumar, A. Dangi, J. A. Antony, S. Dutta, and R. Pratap, "Low cost, contamination-free, and damage-free fabrication of PZT MEMS on SOI substrate," *J. Micromech. Microeng.,* vol. 32, no. 2, Dec. 2021, Art no. 025003, doi: 10.1088/1361-6439/ac4382.

[19] H. Wang, H. Yang, Z. Chen, Q. Zheng, H. Jiang, P. X. L. Feng, H. Xie, "Development of Dual-Frequency PMUT Arrays Based on Thin Ceramic PZT for Endoscopic Photoacoustic Imaging," *J. Microelectromech. Syst.,* vol. 30, no. 5, pp. 770-782, Oct. 2021, doi: 10.1109/jmems.2021.3096733.

[20] H. Tian, J. Liu, B. Dong, J. C. Skehan, M. Zervas, T. J. Kippenberg, S. A. Bhave, "Hybrid integrated photonics using bulk acoustic resonators," *Nat. Commun.,* vol. 11, no. 1, Jun. 2020, Art no. 3073, doi: 10.1038/s41467-020-16812-6.

[21] V. J. Gokhale, B. P. Downey, D. S. Katzer, N. Nepal, A. C. Lang, R. M. Stroud, D. J. Meyer, "Epitaxial bulk acoustic wave resonators as highly coherent multi-phonon sources for quantum acoustodynamics," *Nat. Commun.,* vol. 11, no. 1, May 2020, Art no. 2314, doi: 10.1038/s41467-020-15472-w.

[22] L. Shao, V. J. Gokhale, B. Peng, P. Song, J. Cheng, J. Kuo, A. Lal, W. M. Zhang, J. J. Gorman, "Femtometer-amplitude imaging of coherent super high frequency vibrations in micromechanical resonators," *Nat. Commun.,* vol. 13, no. 1, Feb. 2022, Art no. 694, doi: 10.1038/s41467-022-28223-w.